

# Persistent Weak Interferer Detection for WiFi Networks: A Deep Learning Based Approach

Andrew Adams, Richard F. Obrecht, Miller Wilt,  
Daniel Barcklow, Bennett Blitz, Daniel Chew

The Johns Hopkins University Applied Physics Laboratory

**Abstract**—In this paper, we explore the use of multiple deep learning techniques to detect weak interference in WiFi networks. Given the low interference signal levels involved, this scenario tends to be difficult to detect. However, even signal-to-interference ratios exceeding 20 dB can cause significant throughput degradation and latency. Furthermore, the resultant packet error rate may not be enough to force the WiFi network to fallback to a more robust physical layer configuration. Deep learning applied directly to sampled radio frequency data has the potential to perform detection much cheaper than successive interference cancellation, which is important for real-time persistent network monitoring. The techniques explored in this work include maximum softmax probability, distance metric learning, variational autoencoder, and autoregressive log-likelihood. We also introduce the notion of generalized outlier exposure for these techniques, and show its importance in detecting weak interference. Our results indicate that with outlier exposure, maximum softmax probability, distance metric learning, and autoregressive log-likelihood are capable of reliably detecting interference more than 20 dB below the 802.11 specified minimum sensitivity levels. We believe this presents a unique software solution to real-time, persistent network monitoring.

**Index Terms**—Anomaly detection, artificial neural networks, autoregressive, bit error rate, deep learning, distance learning, electromagnetic interference, information entropy, NOMA, OFDM, packet loss, radio spectrum monitoring, statistical distribution, statistical learning, wireless LAN

## I. INTRODUCTION

WIRELESS connectivity has become ubiquitous in modern society. This is illustrated by the vast amounts of internet traffic we produce. In 2020, global internet traffic reached an average of 175 exabytes per month, and is expected to reach 300 exabytes per month by 2022 [1]. This is an enormous amount of data being trafficked, which indicates the level of integration internet access has in our daily lives. Although our consumption of wireless services continues to increase, spectrum regulations have lagged in supporting the increased traffic rates [2]. Nowhere is this more evident than the unlicensed Industrial, Scientific, and Medical (ISM) frequency bands, where WiFi is forced to operate. Here WiFi competes with itself (co-located networks) and other popular wireless standards for spectrum access. These include Long Term Evolution License Assisted Access (LTE-LAA), Bluetooth, ZigBee, cordless phones, radio frequency identification (RFID) tags, and many proprietary wireless devices and protocols. As such, the ability to detect and mitigate sources of interference is central to any successful WiFi network deployment.

*Interference* occurs when WiFi transmissions collide with other traffic attempting to use the same or adjacent overlapping channels. This induces various signal processing errors within the intended receiver resulting in reduced network throughput and increased network latency. As discussed in Ref. [3], even relatively weak levels of interference can severely degrade WiFi network performance. The authors demonstrate a significant reduction in throughput and an increase in latency with signal-to-interferer (SIR) ratios as large as 20 dB. However, these can be the most difficult to detect from a network mon-

itoring perspective, whereby the necessary mitigation strategy is never initiated.

In this paper, we explore multiple deep learning (DL) methods to enable persistent detection of weak interferers. Our motivation to explore DL for this application is twofold. First, detection of weak interferers enables network administrators to execute appropriate mitigation strategies, either manually or autonomously, with the most effective being frequency agility [3]. Furthermore, given the consistent use of WiFi to facilitate internet traffic, a persistent monitoring capability can run 24/7, and alert network administrators only when mitigation is required.

Second, DL has the potential to provide a persistent monitoring capability at a fraction of the computational cost of existing techniques, including successive interference cancellation (SIC) [4]. When employing SIC, any unwanted traffic is first demodulated to determine content, re-modulated, and then subtracted from the input sample stream. The resulting residue is then analyzed for indications of desired signal traffic or potential signals of interest (SOI). This is a highly complex process, where the performance depends heavily upon accurate estimates of both hardware and channel impairments by the intended receiver. This process is discussed at length in Ref. [5], where in-phase/quadrature (IQ) imbalance, direct current (DC) offset, and power amplifier (PA) non-linearities are shown to reduce the performance of non-orthogonal multiple-access (NOMA) communications systems. Another example is the bit error rate (BER) floor induced by uncompensated transmitter windowing in orthogonal frequency division multiplexing (OFDM) communications systems [6].

Given these motivating factors, we demonstrate the use of

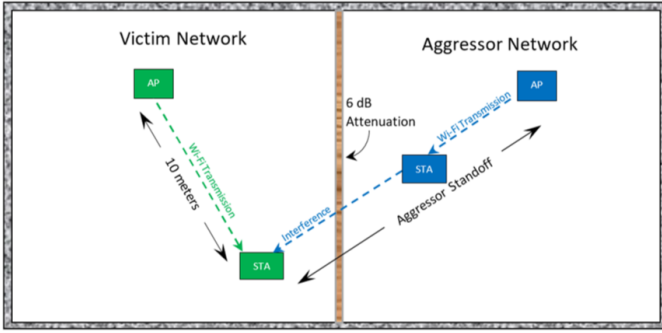


Fig. 1: An example of a co-channel interference scenario.

received sample stream without the need for SIC or any other unwanted signal removal or impairment compensation.

## II. EXPERIMENT SETUP

For experimentation purposes, we chose to replicate the common occurrence of co-channel interference caused by frequency reuse of wireless local area network (WLAN) channels between co-located WiFi networks. This scenario is illustrated in Figure 1, where two simple networks, each consisting of a single access point (AP) and wireless station (STA), are separated geographically but attempt traffic exchange on the same WLAN channel. The *victim* network is so named because in this scenario it began traffic exchange on a particular WLAN channel first; the *aggressor* network is so named because in this scenario it began traffic exchange on the same WLAN channel at some point thereafter. Victim and aggressor roles hold relative meaning only, and could be reversed at any time.

In this scenario, the aggressor network operates in close proximity, such as an adjacent office space or outdoor block. As the aggressor network begins traffic exchange, the victim STA experiences co-channel interference; the magnitude of which depends upon the aggressor STA transmit power, standoff, and signal attenuation due to intervening walls or partitions. Assuming a victim AP power level of +20 dBm, aggressor STA transmit power levels ranging from 0 dBm to +20 dBm, aggressor STA standoffs ranging from 1 m to 100 m, and 6 dB partition loss, Figure 2 shows the resultant signal-to-interference ratios (SIR) at the victim STA. These levels suggest the victim STA packet error rates (PER) may not exceed 10%, which means the co-channel interference may not be enough to force it to a lower modulation coding scheme (MCS) [7]. However, as demonstrated in Ref. [3], it is certainly enough to reduce victim network throughput and quality of service (QoS). Hence our desire to pursue detection methods relevant to *weak* interferers.

We therefore explore the ability of select DL techniques to detect weak interferers for various static MCS values. Assuming a victim STA OFDM physical layer (PHY) configuration, Ref. [7] specifies the minimum required receiver sensitivity for each MCS value. Assuming the noise figure and implementation loss specified there, room temperature, and a noise bandwidth of 20 MHz, we can derive the minimum

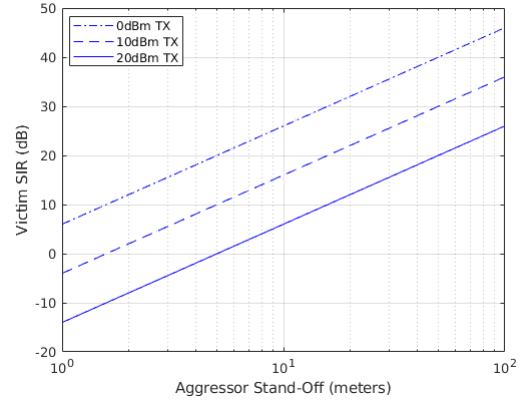


Fig. 2: Victim STA interference levels as a function of aggressor distance.

specified operating signal-to-noise ratio,  $\text{SNR}_{\min}(\text{dB})$ , for each subcarrier modulation type specified. These include binary phase shift keying (BPSK), quadrature phase shift keying (QPSK), and quadrature amplitude modulation (QAM) as listed in Table I. For our experiments, SNR and SIR are combined into a metric termed **signal-to-interference-and-noise ratio (SINR)**. Since the interference level is not enough to force the victim STA to a lower MCS value, the SINR is assumed to include an SIR range between  $\text{SNR}_{\min}(\text{dB})$  and  $\text{SNR}_{\min} - 20$  dB when present. This is expressed mathematically as

$$\begin{aligned} \text{SINR} &= 10^{-\text{SNR}_{\min}/10} \\ &= 10^{-\text{SIR}/10} + 10^{-\text{SNR}/10}, \end{aligned} \quad (1)$$

where  $\text{SNR}_{\min}$  is defined in Table I. SIR is drawn from a uniform distribution  $\in [10^{\frac{-\text{SNR}_{\min}-20}{10}}, 10^{\frac{-\text{SNR}_{\min}}{10}}]$ , and SNR consumes the difference. The result is a range of continuous SINR values dominated by SIR or SNR on either extreme. The outcome of each experiment is thus the quantitative measure of our ability to use DL to accurately detect co-channel interference at a given SIR when present.

## III. RELEVANT WORKS

To our knowledge, our DL based approach to weak interferer detection is novel. However, relevant performance and complexity comparisons can be made to multiple access schemes employing SIC. Briefly, SIC allows multiple transmitters to occupy a common channel simultaneously. At the receiver, any unwanted traffic is first demodulated, re-modulated, and then subtracted from the input sample stream. To do so, the desired traffic is treated as co-channel interference

TABLE I: Minimum SINR per subcarrier modulation type.

Modulation	$\text{SNR}_{\min}$ (dB)
BPSK	3.92
QPSK	6.92
16-QAM	11.92
64-QAM	19.92

while demodulating the undesired traffic; hence our basis for comparison. Finally, the desired traffic is then recovered from the resulting residue when present. For packetized transmissions, this is done in *succession* to recover the entire message, hence the term *successive interference cancellation*. We do not present a quantitative analysis of relative complexity here, as that entails algorithmic implementation details for either approach. We do however highlight relevant works discussing current perceived limitations of SIC as motivation to explore other approaches.

Ref. [4] discusses the medium access control (MAC) layer throughput gains provided by SIC as compared to a time sharing approach such as time division multiple access (TDMA). Their conclusion is that throughput gains are marginal for distinct transmitter-receiver pairs. That is, as a means to combat co-channel interference, SIC provides little to no benefit. The reason being that for SIC to be feasible, certain requirements regarding transmitter bit rates and signal strength must be met. For multiple transmitters and a common receiver, SIC then provides modest gains as the transmitters can coordinate to meet said feasibility requirements.

Ref. [4] assumes perfect cancellation, which is of course unobtainable. Ref. [5] illuminates this challenge while discussing performance degradation within NOMA schemes due to RF front-end impairments; NOMA relies heavily upon SIC to eliminate multi-user interference. To minimize receiver complexity, impairments such as IQ imbalance, DC offset, and PA non-linearities are often ignored. While these often have little effect on TDMA schemes, these present significant performance degradation to NOMA schemes in the form of imperfect cancellation. Ref. [6] discusses a similar concern with OFDM windowing techniques, which are often not standardized or known a priori by the intended receiver.

#### IV. DEEP LEARNING BASED APPROACHES

In this work, we demonstrate detection of weak interferers using various deep learning approaches. Deep learning is a form of representation learning, where complex concepts are built from combinations of simpler ones [8]. These are commonly implemented using artificial neural networks with numerous hidden layers, *i.e.* deep, where each layer tends to learn different features from the preceding layers. This results in a specific concept being learned by iteratively traversing the network, depth-wise, as part of an optimization algorithm, such as stochastic gradient descent. Once trained, the inferred network approximates a function that produces the desired output from a given input, and can be expressed mathematically as  $y = f(x)$ , where  $f(x)$  is not limited to linear functions. Deep learning has been shown adept in performing various learning tasks across many disciplines and applications. Examples related to wireless communications include modulation recognition directly from baseband samples [9–11] and reinforcement learning Q-function approximation for network resource scheduling [12, 13]. We experiment with deep anomaly detection as a means to detect weak co-channel interference within WiFi networks. As such, we train neural networks to produce multiple feature representations and

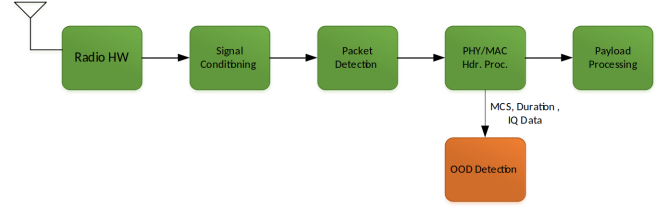


Fig. 3: An OOD detection application.

anomaly scores indicative of situations where weak interferers may be reducing network throughput or inducing additional traffic latency.

For the interested reader, Ref. [14] provides a comprehensive review of deep anomaly detection methods. We instead focus on a closely related form of deep anomaly detection called **out-of-distribution** (OOD) detection, which is attractive for this application because it enables anomaly detection in an open-world scenario; that is, we assume we have sufficient labeled examples of what normal looks like, but make no assumptions with respect to the types of anomalies encountered once deployed. As such, **in-distribution** (ID) refers to the traffic exchanged between nodes within our own network without any weak interferers present; OOD then refers to similar traffic exchange, but in the presence of weak co-channel interference.

Since we are processing baseband (IQ) samples directly, normal necessarily depends upon the various network physical layer configurations. Since this is an in-network monitoring application, we assume we can detect each packet and recover the PHY and MAC headers such that the MCS and packet duration are known prior to network inference. This reduces the scope of our experiments to OOD detection, and prevents the detection algorithms from processing noise only. Figure 3 illustrates how this application may be deployed alongside regular traffic processing on a given observation node or AP.

Note that other published works, including Refs. [14–16], distinguish OOD detection from other anomaly detection methods by the capability to do so alongside primary learning tasks such as classification. While we believe this to be beneficial, it is not the focus of our experimentation. However, future work may include this capability to detect weak interferers with little to no header information. This would certainly be attractive when attempting to monitor WiFi networks without first joining the network being monitored.

##### A. Out of Distribution Detection

OOD refers to examples drawn from a different distribution than that which are considered to be ID or normal [14–17]. Detecting OOD examples can be done by training deep neural networks to generate various representations or metrics of the input data, which adequately differ between OOD and ID examples. However, for OOD examples to be detected within an open-world deployment scenario, we can make no assumptions regarding the types of anomalies during network inference. Since that is our goal here, we focus on (4) specific methods of OOD, assuming only the availability of labeled

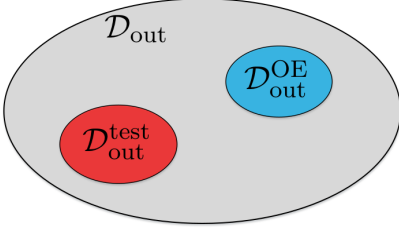


Fig. 4: Illustrating the various OOD notations used throughout the text.

ID training data: **maximum softmax probabilities (MSP)**, **distance metric learning (DML)** similarity scores, **variational autoencoder (VAE)** reconstruction loss, and **autoregressive (AR)** model likelihood. We elaborate on each method following an introduction to outlier exposure.

## B. Outlier Exposure

### 1) Motivation

While many OOD detection models detect anomalies using learned representations of ID examples only, an auxiliary OOD dataset may be used to learn heuristics of OOD examples, a technique known as outlier exposure (OE) [16]. This is motivated by the use of complex datasets, where anomalies are difficult to detect, which is particularly of concern here given the diversity of WiFi signal formats. Hendrycks *et al.* represent outliers using disjoint datasets  $\mathcal{D}_{in}$  and  $\mathcal{D}_{out}^{OE}$ ; that method is not applicable here as each anomalous example still represents a valid class. In fact, one may find parallels between this application and the notion of domain shift as discussed in Ref. [17]. Unfortunately, we do not have the same benefit of using multiple examples to detect weak interferers as that has the potential to introduce significant latency into our monitoring system. We still utilize OE to train our networks to be sensitive to the presence of weak interferers; however, our outliers must be representative of relatively weak co-channel interference.

Given  $x$  drawn from an ID dataset  $\mathcal{D}_{in}$ , a class label  $y$ ,  $x'$  drawn from an OOD dataset  $\mathcal{D}_{out}^{OE}$ , a model  $f$ , and the original learning objective  $\mathcal{L}$ , outlier exposure is defined by minimizing the following objective:

$$\mathbb{E}_{(x,y) \sim \mathcal{D}_{in}} \left[ \mathcal{L}(f(x), y) + \lambda \mathbb{E}_{x' \sim \mathcal{D}_{out}^{OE}} [\mathcal{L}_{OE}(f(x'), f(x), y)] \right], \quad (2)$$

where  $\lambda$  is a scaling factor and  $\mathcal{L}_{OE}$  is a function of  $f(x')$ ,  $f(x)$ , and  $y$ . In other words, the process is to first maximize the classification accuracy using data drawn from  $\mathcal{D}_{in}$ , and then to minimize confidence using data drawn from  $\mathcal{D}_{out}^{OE}$ .

Note that the complete set of out-of-distribution samples is represented by  $\mathcal{D}_{out}$ , which is difficult or impossible to know *a priori*. When applying OE to training procedures, we are intending to parametrize a subset of  $\mathcal{D}_{out}$ , labeled as  $\mathcal{D}_{out}^{OE}$ . During testing, another subset of OOD samples that are different from  $\mathcal{D}_{out}^{OE}$  is introduced, and is defined to be  $\mathcal{D}_{out}^{test}$ . The nuances in notation are illustrated by Figure 4.

### 2) Signal Model

Examples exhibiting weak interference still primarily represent valid classes. As such, the use of disjoint data sets in Ref. [16], or the sample replacement strategy in Ref. [18], are not applicable here. We therefore need to define OE for OFDM signals experiencing co-channel interference.

The continuous time OFDM signal  $r(t)$  is described by

$$r(t) = \mathcal{A} \sum_{k=0}^{K-1} \sum_{l=-\infty}^{\infty} s_{k,l} e^{j2\pi k \delta f_k (t-lT-\epsilon T)} g(t-lT-\epsilon T) + n(t), \quad (3)$$

where  $\mathcal{A} = ae^{j\theta} e^{j2\pi \delta f_c t}$ ,  $K$  is the number of subcarriers,  $\delta f_k$  is the subcarrier spacing,  $T$  is the OFDM symbol period, and  $s_{k,l}$  is the modulation symbol value for the  $k_{th}$  subcarrier of the  $l_{th}$  OFDM symbol. The function  $g(t)$  is the pulse shape resulting from any transmit or receive filtering, and  $n(t)$  represents zero-mean, complex additive Gaussian noise.  $a$ ,  $\delta f_c$ , and  $\epsilon$  are the power factor, carrier frequency offset, and time offset, respectively. In the presence of co-channel interference  $I(t)$ , Eqn 3 may be rewritten as

$$r_{OE}(t) = \mathcal{A} \sum_{k=0}^{K-1} \sum_{l=-\infty}^{\infty} s_{k,l} e^{j2\pi k \delta f_k (t-lT-\epsilon T)} g(t-lT-\epsilon T) + n(t) + I(t), \quad (4)$$

where  $\mathcal{A} = ae^{j\theta} e^{j2\pi \delta f_c t}$ . The goal now is to select a model for  $I(t)$ , which will serve as  $\mathcal{D}_{out}^{OE}$  for OE purposes.

Recall our constraint of making no assumptions about the types of interference encountered; we desire our OE to generalize to a broad class of co-channel interference. For inspiration, we look to the OFDM jammer effectiveness models discussed in Ref. [19]. There, Luo *et al.* compare the effect of multiple interference models on OFDM receiver BER under varying channel conditions and SIR. Their conclusion was that multi-tone interference (MTI) was more effective than either barrage noise interference (BNI) or partial band interference (PBI) under additive white Gaussian noise (AWGN). Furthermore, MTI makes no attempt to model a specific waveform or protocol, and provides enough configuration flexibility to model both co-channel and adjacent channel interference. We therefore model  $I(t)$  as

$$I(t) = a_i \sum_{j=1}^J e^{2\pi f_j t + \phi_j}, \quad (5)$$

where  $a_i$  is the power factor,  $f_j$  is the frequency of the  $j_{th}$  tone, and  $\phi_j$  is the phase of the  $j_{th}$  tone drawn from a uniform distribution over  $[0, 2\pi]$ .

The fraction of tones overlapping OFDM subcarriers is defined as  $\rho = q/K$ , where  $q$  is drawn from a uniform distribution over  $[\frac{K}{8}, K]$ ; these were chosen to represent the continuum between partial and full overlap with each OFDM symbol in the spectrum. Note that we have no requirement for  $J$  to be a contiguous set of integers with respect to  $K$  or otherwise.



### C. Maximum Softmax Probability

As discussed above, several works derive an OOD detection capability from a primary task, such as classification. MSP, developed by Hendrycks and Gimpel, is an effective OOD baseline built on top of classification models [15]. Specifically, this approach utilizes the predicted (*i.e.*, maximum) softmax score to determine if a given example is ID or OOD. The authors demonstrate that while deep neural networks are overconfident in their predictions, even those generated from OOD data, the scores from OOD data are generally lower than scores from ID data. This enables the detection of OOD data via a surprisingly simple, but effective method: just compare the softmax score of a given example to prediction statistics generated from a set of known ID data.

Unlike many of the classification-based OOD detection works, our primary goal is to determine if an example is ID or OOD, not to classify it. However, given that MSP is built on top of a classification model, we must create an auxiliary classification task to enable its use. We take the approach of classifying the (4) OFDM physical layer subcarrier modulation types discussed in Section II. However, given the strong similarity between ID and OOD signal traffic, we add outlier exposure to make this approach more sensitive to weak interferers.

#### 1) Outlier Exposure

We leverage the OE approach for multiclass classification as described in Ref. [16], where  $\mathcal{L}_{\text{OE}}$  is defined as the cross-entropy between the softmax scores of the outlier data and a uniform distribution. Theoretically (and as we demonstrate below, empirically), this results in the model being less confident when classifying signals with weak interferers present.

#### 2) Implementation

For experimentation purposes, we utilize a modified pre-activation ResNet-34 [20, 21] architecture, which we describe here. First, all 2D convolutions are replaced with 1D convolutions to handle the shape of the signal data. Second, similar to Ref. [22], dropout [23] is included in each residual block right before the second convolutional layer. Lastly, all strided convolutions are removed and replaced with dilated convolutions [24]. We take inspiration from the approach described in Ref. [25] and increase the dilation factor by a power of two with each residual block up to a factor of 128 before repeating.

### D. Distance Metric Learning

DML attempts to learn a distance consistent with semantic similarity [26]. In other words, a network is trained to generate representations in an embedding space, where inputs drawn from the same class or distribution are close to each other, but also separated from those drawn from a different class or distribution. The relevant task here is to learn an embedding representing normal network traffic, which is separable from that experiencing weak co-channel interference. Ref. [27] introduced the triplet loss, which optimized the relative distance between select triples consisting of an anchor and both positive (similar) and negative (dissimilar) examples. Ref. [26]

introduced the proxy-NCA loss, which improved upon triplet-loss performance and convergence rates by utilizing proxies for entire subsets of training data. We utilize the proxy-anchor loss [28], which takes advantage of both the data-to-data relations described by the triplet loss and the data-to-proxy relations described by the proxy-NCA loss.

The proxy-anchor loss is defined as

$$\ell(X) = \frac{1}{|P^+|} \sum_{p \in P^+} \log \left( 1 + \sum_{x \in X_p^+} e^{-\alpha(s(x,p)-\delta)} \right) + \frac{1}{|P|} \sum_{p \in P} \log \left( 1 + \sum_{x \in X_p^-} e^{\alpha(s(x,p)+\delta)} \right), \quad (6)$$

where  $P$  is the set of all proxies,  $P^+$  is the set of positive proxies within a given batch of data,  $X_p^+$  is the set of positive embedding vectors for proxy  $p$ , and  $X_p^-$  is the disjoint set  $X - X_p^+$ . Using the cosine similarity  $s$  between embeddings  $x$  and  $p$ ,  $\ell$  decreases when  $x \in X_p^+$  is close to  $p \in P^+$ , and increases otherwise. As a result,  $p$  and its positive examples are pulled closer together, while  $p$  and its negative examples are pushed further apart. The proxies are learned while training [26], and  $\alpha$  and  $\delta$  are used for scaling and margin, respectively.

Using proxy-anchor loss, we can train a network to learn unique embeddings representing normal network traffic for each of the valid subcarrier modulation types. This becomes a classifier-based training approach, where the (4) classes are defined in Table I. However, given the relatively weak interference levels we expect to identify for this application, we utilize OE during training to make the trained network sensitive to weak interferers.

#### 1) Outlier Exposure

For our application, we seek to learn unique embeddings for the (4) classes representing valid subcarrier modulation types and the (4) classes representing valid subcarrier modulation types experiencing weak interference. This results in (8) classes total, with a single classifier-based learning objective utilizing the proxy-anchor loss. Therefore, Eqn 2 may be reformulated as

$$\mathbb{E}_{(x,y) \sim D_{\text{in}}, D_{\text{out}}^{\text{OE}}} [\mathcal{L}(f(x), y)], \quad (7)$$

where  $\mathcal{L}$  is defined by Eqn 6.

#### 2) OOD Score

An OOD metric is based on the distance between embeddings representing normal network traffic and those experiencing weak interference. Each embedding  $\in \mathbb{R}^d$ , where  $d$  is the number of dimensions, *e.g.* 64, 128, 256, etc. Many distance metrics however lose meaning as  $d$  increases. For example, Ref. [29] attempts to mitigate this limitation through the use of fractional distance metrics. Cosine similarity does not have the same limitation, but substantial information may be lost when calculating the similarity between each embedding and its mean values only. We therefore look to model the probability density function (PDF) of each dimension in order to fully characterize normal behavior. Since each dimension has no incentive to strictly follow a normal distribution, each

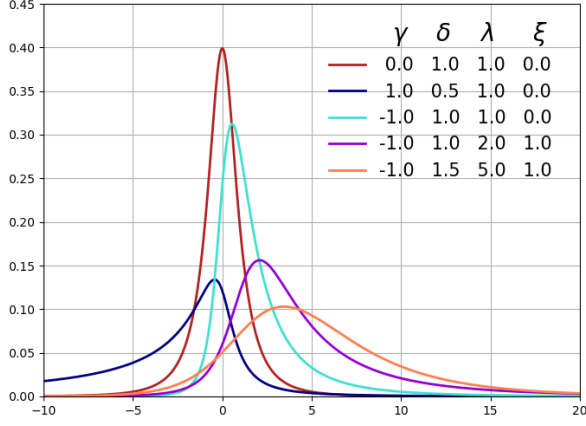


Fig. 5: Various examples of the Johnson SU PDF.

dimension is modeled as an unbounded Johnson distribution (Johnson SU) with the following PDF:

$$f(x) = \frac{\delta}{\lambda \sqrt{2\pi} \sqrt{z^2 + 1}} e^{-\frac{1}{2}(\gamma + \delta \sinh^{-1} z)^2}, \quad (8)$$

where  $z$  is parametrized as  $\frac{x-\xi}{\lambda}$ ,  $\xi$  is a location parameter,  $\lambda$  is a scaling parameter, and  $\gamma$  and  $\delta$  are shape parameters [30]. The Johnson SU PDF is capable of modeling various asymmetric distributions; see Figure 5, where each curve represents the indicated  $(\gamma, \delta, \lambda, \xi)$  tuple.

### 3) Implementation

For experimentation purposes, we utilize a ResNet-34 [21] architecture, but with the convolution operations replaced by the dilated convolution operation [24]. These expand the receptive field without loss of resolution. Since we are operating on complex data, the I and Q components of each sample are separated and placed in separate input channels, similar to the separate R, G, and B channels utilized for image processing. The ResNet output is pooled and flattened, and a dropout of 0.25 applied. The result is then run through a dense layer with an output width equal to our desired embedding size of 128. Training is performed using AdamW [31] optimization and a cosine annealing [32] period of 10.

### E. Variational Autoencoder

A variational autoencoder (VAE) [33] is a popular unsupervised learning technique, and is capable of generating or reconstructing examples similar to the input. The model is trained on signals that are considered normal or expected. In inference mode, when the model is given a signal experiencing a weak interferer, the reconstruction should be relatively poor, allowing for a method of detection. The loss metric for a traditional autoencoder is often the mean squared error between the input  $x$  and the reconstructed output  $\hat{x}$ . The variational approach, however, encodes the inputs as probability distributions, which regularizes the latent space by constraining each dimension to be approximately Gaussian. The decoder then samples the latent space to generate new noisy examples; sampling is used to overcome the overfitting nature of conventional autoencoders. The mathematical details

of VAEs are summarized below; see Refs. [33–37] for more information.

A VAE is a continuous latent variable model. An unobserved latent representation  $z$  is used to generate an observation  $x$ . The probability distribution  $p_\theta(x|z)$ , parameterized by  $\theta$ , describes the process of generating  $x$  from a lower-dimensional representation  $z$  described by prior  $p(z)$ . Assuming the latent probability distribution  $p(z)$  is known, the goal is to learn the marginal likelihood of the data:

$$\max_{\phi, \theta} \mathbb{E}_{q_\phi(z|x)} [\log p_\theta(x|z)], \quad (9)$$

which may be rewritten as

$$\log p_\theta(x|z) = D_{\text{KL}}(q(z|x) || p(z)) + \mathcal{L}(\theta, \phi; x, z), \quad (10)$$

where  $\phi, \theta$  parameterize the the encoder and decoder distributions respectively. The  $D_{\text{KL}}(||)$  term is the non-negative Kullback-Leibler (KL) divergence between the true and approximate posterior. To make the optimization tractable,  $\mathcal{L}(\theta, \phi; x, z)$  is maximized:

$$\log p_\theta(x|z) \geq \mathcal{L}(\theta, \phi; x, z) = \mathbb{E}_{q_\phi(z|x)} [\log p_\theta(x|z)] - D_{\text{KL}}(q(z|x)||p(z)) \quad (11)$$

where the prior  $p(z)$  and posterior  $q_\phi(z|x)$  are approximated as Gaussian. Rewritten more simply, the VAE loss is

$$\mathcal{L}_{\text{VAE}} = \mathcal{L}_{\text{MSE}} + \beta \mathcal{L}_{\text{KL}}, \quad (12)$$

where  $\mathcal{L}_{\text{MSE}} \equiv \mathbb{E}_{q_\phi(z|x)} [\log p_\theta(x|z)]$  is commonly taken as the mean squared error between the input  $x$  and the output  $\hat{x}$ , and  $\mathcal{L}_{\text{KL}}$  has an analytical form under Gaussian assumptions. The empirical factor  $\beta$  is often introduced to scale  $\mathcal{L}_{\text{KL}}$ , referred to as a  $\beta$ -VAE. As  $\beta \rightarrow 0$ , the VAE reduces to the traditional deterministic autoencoder. Increasing the value of  $\beta$  has been motivated to further constrain the capacity of the encoder in order to allow a more factorized latent representation [38, 39].

#### 1) Outlier Exposure

The goal is to minimize  $\mathcal{L}_{\text{VAE}}$  using ID data while simultaneously maximizing a loss associated with outlier exposure, defined to be  $\mathcal{L}_{\text{OE}}$ , which utilizes both ID and OOD data. OE is incorporated into Eqn 12 as a penalty term:

$$\mathbb{E}_{x \sim \mathcal{D}_{\text{in}}} \mathcal{L}_{\text{VAE}}(x) + \lambda \mathbb{E}_{x \sim \mathcal{D}_{\text{in}}, x' \sim \mathcal{D}_{\text{out}}^{\text{OE}}} \mathcal{L}_{\text{OE}}(x, x'), \quad (13)$$

where  $\lambda$  is a scaling factor,  $\mathcal{D}_{\text{in}}$  represents the ID dataset, and  $\mathcal{D}_{\text{out}}^{\text{OE}}$  represents the OOD dataset used during training. The loss function with the OE modification is

$$\mathcal{L} = \mathcal{L}_{\text{VAE}} - \lambda \mathcal{L}_{\text{OE}}, \quad (14)$$

where  $\mathcal{L}_{\text{OE}}$  may be calculated using the approaches described in Ref. [37]. We choose to calculate  $\mathcal{L}_{\text{OE}}$  using the input  $x$  and the corresponding reconstructed output  $\hat{x}$ :

$$\mathcal{L}_{\text{OE}} = \sigma(\text{MSE}_{\text{OOD}}(x', \hat{x}') - \text{MSE}_{\text{ID}}(x, \hat{x})), \quad (15)$$

where  $\sigma$  is the typical sigmoid function, and  $x$  and  $x'$  live in  $\mathcal{D}_{\text{in}}$  and  $\mathcal{D}_{\text{out}}^{\text{OE}}$ , respectively. Eqn 14 wants to reconstruct ID data well, while poorly reconstructing OOD data.

## 2) Implementation

The encoder is used to build two latent representations, one each for I and Q separately. Then, two identical decoding networks are used to regenerate both I and Q, which are then concatenated to reconstruct the complex input. The encoder block is constructed out of strided convolutional layers followed by batch normalization and a ReLU activation function. It is relatively shallow, built from only two encoding blocks, which effectively reduces the IQ input length by a factor of four while increasing the channel dimension by a factor of four. A flattening operation is then performed to create the latent linear layer, which funnels the encoding features from 512 to an empirically determined size of 128. The decoder is symmetric to the encoder, but uses strided transpose convolutional layers.

## F. Autoregressive Log Likelihood

Deep autoregressive models are a form of generative model that learn a distribution over a given input space. Unlike many other generative models, *e.g.*, GANs and VAEs, autoregressive models produce a tractable likelihood for a given input. Specifically, the joint probability of each input  $\mathbf{x} = \{x_1, \dots, x_T\}$  is factorized into a product of conditional probabilities:

$$p(\mathbf{x}) = \prod_{t=1}^T p(x_t | x_1, \dots, x_{t-1}). \quad (16)$$

Stated another way, each input element  $x_t$  is conditioned on all data from previous time steps. Traditionally, these conditional probability distributions are modeled using either recurrent neural networks (*e.g.*, PixelRNN [40]) or convolutional neural networks (*e.g.*, PixelCNN, WaveNet [25, 40]), the latter trading an unbounded receptive field for reduced computation cost at training due to parallelization.

Using generative models for anomaly detection is a well established approach [41], and deep autoregressive models are especially appealing for anomaly detection since they can tractably compute the likelihood of complex inputs. Similar to the MSP method, this theoretically<sup>1</sup> facilitates the detection of OOD data by just comparing the computed likelihood of a given example to likelihood statistics generated from a set of known ID data. As in our other methods, we make use of outlier exposure to make this approach more sensitive to weak interferers.

### 1) Outlier Exposure

We leverage the OE approach for density estimation as described in Ref. [16], where  $\mathcal{L}_{\text{OE}}$  is defined as the margin loss over the log-likelihood difference between ID and OOD data:

$$\mathcal{L}_{\text{OE}} = \max(0, m + \text{NLL}(f_{\theta}(x)) - \text{NLL}(f_{\theta}(x'))), \quad (17)$$

where  $f_{\theta}$  is a neural network with parameters  $\theta$ , NLL is the negative log-likelihood,  $x$  and  $x'$  are ID and OOD examples respectively.  $m$  is a margin hyperparameter.

<sup>1</sup>Recently, Nalisnick *et al.* demonstrated that deep generative models often assign higher likelihoods to OOD data compared to ID data [42]; however, we find our model does not suffer from this problem. We hypothesize this may be due to the similarity of our ID and OOD data.

## 2) Implementation

The autoregressive model is based on temporal convolutional networks (TCNs), a family of architectures for sequence modeling tasks [43]. TCNs are inspired by the WaveNet architecture [25] while being less complex to implement. Like WaveNet, they make use of appropriate zero padding and causal convolutions to ensure the model is autoregressive in nature. In this work, we eschew the original architecture developed in Ref. [43] and instead use building blocks common to our other methods to enable a fairer comparison. Specifically, the 1D ResNet-34 architecture developed in the MSP and DML methods is used as the TCN backbone, modifying all convolutions to be causal. Note that this backbone is not enough by itself, as we must model the conditional probabilities  $p(x_t | x_1, \dots, x_{t-1})$ . To accomplish this, the backbone is connected to a mixture density network (MDN) [44], which models the conditional distributions as a mixture of Gaussians. Note that this is in contrast to the PixelRNN, PixelCNN, and WaveNet architectures, which model the conditional probabilities using a softmax distribution. Through testing, we found that the MDN improved detection performance while providing faster training and inference speed.

## V. EXPERIMENTS

### A. Signal Synthesis

The samples generated for each experiment follow the scenario described in Section II and the signal processing chain described in Section IV. The processing chain, including the OOD detection sub-system, is described in Figure 3. ID samples are generated by following the 802.11 OFDM specification, and represent the nominal case when an aggressor is not currently interfering with the victim STA. At the point in the receive chain where OOD detection takes place, we assume coarse synchronization and equalization have already been achieved; therefore, synchronization error is not considered in this study.

OOD samples are generated in a similar manner as ID samples, except that a weak interfering signal is also added. We test with two different sources of co-channel interference; another 802.11 OFDM signal and an 802.11 DSSS signal. The OFDM interferer is identical in structure to the victim STA OFDM signal described by Eqn 3. The DSSS interferer is a DBPSK DSSS signal carrying a randomly generated payload, and is described as

$$r_{\text{DSSS}}(t) = a e^{j\theta} e^{j2\pi\delta f_c t} s_p x_m g(t - mT), \quad (18)$$

where  $s_p$  represents a pseudo-random spreading sequence of length  $P$ ; the duration of each value is  $T/P$  seconds and can take values of  $\pm 1$  sec. The term  $x_m$  represents each DBPSK symbol of duration of  $T$  seconds, which also takes on values of  $\pm 1$  sec.  $g(t)$  represents the impulse response of any receive or transmit filtering,  $\theta$  is a constant phase offset in the range  $[0, 2\pi)$ ,  $\delta f_c$  is the carrier frequency offset, and  $a$  is a power factor.

As discussed in Section II, the victim STA subcarrier modulation schemes are selected from Table I, which also defines the required SINR. An appropriate SIR is then selected

TABLE II: OOD test dataset notations used during experimentation.

Dataset	Interferer	Apply Channel Effects to Interferer
$(\mathcal{D}_{\text{out}}^{\text{test}})_1$	DSSS	No
$(\mathcal{D}_{\text{out}}^{\text{test}})_2$	DSSS	Yes
$(\mathcal{D}_{\text{out}}^{\text{test}})_3$	OFDM	No
$(\mathcal{D}_{\text{out}}^{\text{test}})_4$	OFDM	Yes

and applied, and the remaining signal power is consumed by SNR. Additionally, the victim and aggressor STAs are not co-located, meaning that each signal experiences different channel effects. Assuming channel equalization in the receiver, corrections made to the desired OFDM signal result in further degradation to the interfering signal. An indoor WLAN TGN channel is used to model degradation to the aggressor STA signal at the receiver.

### B. Dataset Generation

Two of the four datasets described in Section IV-B1 are used to evaluate the performance of our approaches to weak interferer detection:  $\mathcal{D}_{\text{in}}$  and  $\mathcal{D}_{\text{out}}^{\text{test}}$ .  $\mathcal{D}_{\text{in}}$  is used as an ID reference, and the corresponding output considered the nominal ID representation.  $\mathcal{D}_{\text{out}}^{\text{test}}$  contains examples with interferers at varying SIR values. To evaluate the ability of each model to generalize across different types of interferers, each  $\mathcal{D}_{\text{out}}^{\text{test}}$  contains either an 802.11 OFDM interferer or an 802.11 DSSS interferer. To better understand how channel effects to each interferer affects model performance, four datasets are used, and include examples with and without channel effects; see Table II for a summary.

In addition to varying interferer types, detector performance is evaluated with and without OE. Networks trained with OE require additional datasets, labeled  $\mathcal{D}_{\text{out}}^{\text{OE}}$ , which represent cases where parameterized co-channel interference is present; Section IV-B2 provides a detailed description of the MTI-based interferers used during training. Note that the goal is for  $\mathcal{D}_{\text{out}}^{\text{OE}}$  to generalize to  $(\mathcal{D}_{\text{out}}^{\text{test}})_n$ , even though the datasets have distinct signal models sharing minimal physical structure.

The datasets are formatted to have the following dimensions:

$$[\text{Dataset dimensions}] \times [\text{Input sample dimensions}] = \\ [n_{\text{mod}}, n_{\text{sir\_bins}}, n_{\text{batches}}, \text{batch\_size}] \times [\text{block\_size}, n_{\text{channels}}],$$

where the  $n_{\text{mod}}$  dimension supports detector characterization for specific MCS values, allowing us to focus on model performance across various SIR values. To provide detailed detector performance across SIR values, SIR is binned into (14) equi-spaced linear values, annotated by  $n_{\text{sir\_bins}}$ . The variables  $n_{\text{batches}}$  and  $\text{batch\_size}$  represent the number of batches per dataset and number of items per batch, respectively. Lastly,  $\text{block\_size}$  represents the number of complex samples comprising each example, and  $n_{\text{channels}}$  are the real and imaginary components of the complex data.

### C. Inference

To generate a comprehensive set of performance curves, inference results are obtained for all combinations of models

and datasets  $(\mathcal{D}_{\text{out}}^{\text{test}})_n$ . Note that all models take input samples of size  $[960, 2]$  and produce a single inference output score, which represents a metric that is used to flag OOD samples. The eight models used for inference are the four architectures described in this paper, trained both with and without OE. The trained models are listed in Table IV.

For each of the (8) trained models, the  $\mathcal{D}_{\text{in}}$  and each of the four  $\mathcal{D}_{\text{out}}^{\text{test}}$  datasets is provided as input to produce a total of (5) sets of inference output scores per model: (1) set of ID scores and (4) sets of OOD scores. Since there are a total of  $4 \times 14 \times 1024$  input samples per dataset, there are also a total of  $4 \times 14 \times 1024$  inference output scores per dataset. Figure 6 shows the expansion of inference output data for all combinations of models and datasets.

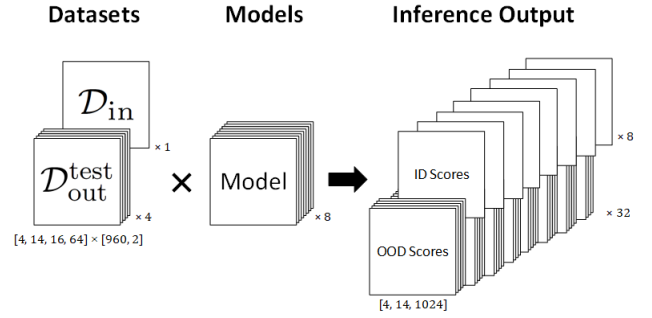


Fig. 6: Combining datasets and models from Tables II and IV for inference.

### D. Evaluation

We define an experiment as the evaluation of performance metrics given a choice of model from Table IV and  $\mathcal{D}_{\text{out}}^{\text{test}}$  from Table II. For each experiment, a set of both ID and OOD inference scores are generated, which are then combined to construct a receiver operating characteristic (ROC) curve. This is an appealing performance metric given that a threshold does not need to be specified, but can be chosen later for a specific operational use-case.

A ROC curve is defined as the relationship between the true positive rate (TPR) and false positive rate (FPR) over a varying threshold. TPR and FPR are calculated as

$$\text{TPR} = \frac{\text{TP}}{\text{TP} + \text{FP}}, \quad \text{FPR} = \frac{\text{FP}}{\text{FN} + \text{TN}}, \quad (19)$$

where TP, TN, FP, FN are the number of true positives, true negatives, false positives, and false negatives, respectively. We

TABLE III: Definitions of dataset dimensions.

Name	Value	Description
$n_{\text{mod}}$	4	number of mod. schemes used by victim STA
$n_{\text{sir\_bins}}$	14	number of SIR bins for plotting
$n_{\text{batches}}$	16	number of batches per SIR bin
$\text{batch\_size}$	64	number of items in a batch
$\text{block\_size}$	960	number of complex signal samples considered
$n_{\text{channels}}$	2	number of channels (real and imaginary)



TABLE IV: The models that have been evaluated.

Model	Section	OE Training	# Parameters
AR	IV-F	No	7556k
AR, OE	IV-F	Yes	7556k
DML	IV-D	No	7250k
DML, OE	IV-D	Yes	7250k
MSP	IV-C	No	7219k
MSP, OE	IV-C	Yes	7219k
VAE	IV-E	No	278k
VAE, OE	IV-E	Yes	278k

define OOD and ID samples to be the positive and negative classes respectively. Since we have discretized the SIR range into 14 bins, there are 14 ROC curves per modulation experiment, where each curve is constructed from 1024 ID and 1024 OOD samples.

The area under the ROC curve (AUROC) metric is used in order to reduce each curve to a scalar performance indicator for ease of comparison across experiments and SIR bins. Since there are  $4 \times 14$  ROC curves generated for each experiment, one for each subcarrier modulation type and SIR bin, there are also  $4 \times 14$  AUROC scores for each experiment. This is further illustrated in Figure 7.

## VI. RESULTS

Figure 8 summarizes the detection performance of each of the DL approaches discussed in Section IV. Each graph plots AUROC scores vs. SIR bin values for one of the subcarrier modulation types listed in Table I. The datasets used to calculate AUROC scores were  $(\mathcal{D}_{\text{out}}^{\text{test}})_2$  and  $(\mathcal{D}_{\text{out}}^{\text{test}})_4$ . Note that each point on each plot represents the area under a single ROC curve generated from 2048 inference scores. Experiments on models trained with OE are plotted as solid lines, and those without OE plotted as dotted lines.

Overall, the AR, DML, and MSP models all perform well with OE applied. For all subcarrier modulation types, each exhibit a monotonically increasing shape as SIR decreases. The DML model does deviate slightly for some QPSK SIR values, but exhibits the best overall performance for 64-QAM. This may be an indication that more than 2048 inference scores are required for each SIR value. The AR model exhibits the least difference in performance between its base model and that with OE applied. The VAE model clearly needs greater SIR levels to reach similar AUROC values, especially for

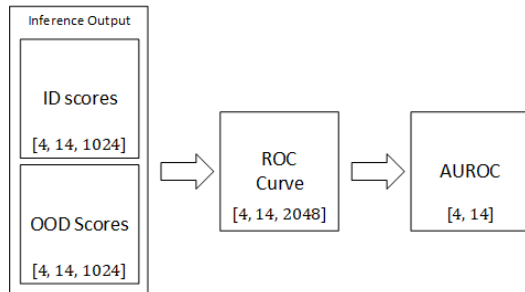


Fig. 7: Combining inference scores in order to evaluate an experiment.

TABLE V: Common training parameters.

Optimizer	AdamW
Weight Decay	0
LR	0.001
Batch Size	64

TABLE VI: Model specific training parameters.

Parameter	AR	DML	MSP	VAE
LR Scheduler	Cosine	CosAnWR	Cosine	CosAnWR
OE Lambda	1.0	N/A	1.0	500.0
OE Margin	1.0	N/A	N/A	2.0
Epochs	50	100	50	100
Batches per Epoch	1024	512	1024	65

higher constellation orders. It also appeared to benefit little from OE. However, given its smaller size as indicated in Table IV, the VAE model may be an appealing approach for resource constrained platforms.

Clearly the DML and MSP models perform much better in this application with OE applied, with the MSP model exhibiting the greatest benefit. Without it, Figure 8 shows two prominent peaks in MSP AUROC scores at various SIR values for both QPSK and 16-QAM subcarrier modulation types. We believe this to be caused by the network's failure at generalizing across perturbations caused by co-channel interference and overconfidence in classifications. Furthermore, this behavior seems to occur at lower SIR values, where perturbations would be at their greatest.

## VII. CONCLUSION

In this work we explored multiple DL approaches to persistent weak interference detection in WiFi networks. We also demonstrated a novel training approach whereby each model is taught the notion of outliers using a generalized signal interference model. The result was the ability to detect weak co-channel and adjacent channel interference at SIR levels at least 20 dB below specified minimum sensitivity levels. As discussed in Ref. [3], this capability has the potential to significantly improve both network throughput and latency. We also suspect this approach can be fielded at a fraction of the computational cost of current techniques, including SIC [4], which is highly susceptible to estimation errors [5] [6]. We suggest exact computational costs of both approaches be the subject of future work in this area.

## APPENDIX

### APPENDIX A: TRAINING PARAMETERS

All models are trained using the AdamW optimizer with batches of size 64. Two types of learning rate schedulers are used: cosine and cosine annealing with warm restarts. Table V shows the list of common training parameters, and Table VI shows training parameters that varied over model architecture. Note that OE lambda and OE margin only apply for models trained with outlier exposure.

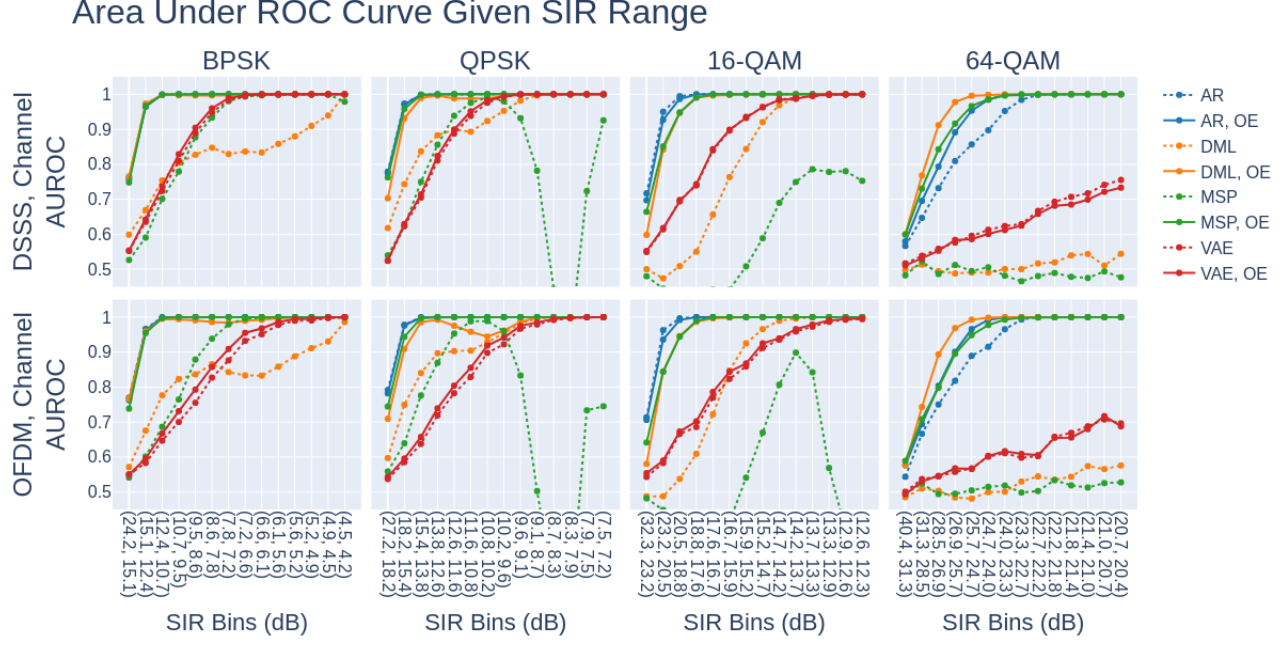


Fig. 8: AUROC scores over SIR bins (dB) for all models and datasets. SIR bins are displayed in descending order to show increase in aggressor STA signal strength relative to victim STA signal strength.

#### APPENDIX B: INTERMEDIATE RESULTS

Figure 9 displays the complete set of ROC curves used to calculate the AUROC scores in the first column of Figure 8, which corresponds to dataset  $(\mathcal{D}_{\text{out}}^{\text{test}})_1$ . The color of each ROC curve describes the SIR bin index. Table VII provides the SIR range for each ROC curve given a bin index and subcarrier modulation type.

TABLE VII: SIR bin ranges (dB) for Figure 9.

Bin Index	BPSK (max, min)	QPSK (max, min)	16-QAM (max, min)	64-QAM (max, min)
1	(24.2, 15.1)	(27.2, 18.2)	(32.3, 23.2)	(40.4, 31.3)
2	(15.1, 12.4)	(18.2, 15.4)	(23.2, 20.5)	(31.3, 28.5)
3	(12.4, 10.7)	(15.4, 13.8)	(20.5, 18.8)	(28.5, 26.9)
4	(10.7, 9.5)	(13.8, 12.6)	(18.8, 17.6)	(26.9, 25.7)
5	(9.5, 8.6)	(12.6, 11.6)	(17.6, 16.7)	(25.7, 24.7)
6	(8.6, 7.8)	(11.6, 10.8)	(16.7, 15.9)	(24.7, 24.0)
7	(7.8, 7.2)	(10.8, 10.2)	(15.9, 15.2)	(24.0, 23.3)
8	(7.2, 6.6)	(10.2, 9.6)	(15.2, 14.7)	(23.3, 22.7)
9	(6.6, 6.1)	(9.6, 9.1)	(14.7, 14.2)	(22.7, 22.2)
10	(6.1, 5.6)	(9.1, 8.7)	(14.2, 13.7)	(22.2, 21.8)
11	(5.6, 5.2)	(8.7, 8.3)	(13.7, 13.3)	(21.8, 21.4)
12	(5.2, 4.9)	(8.3, 7.9)	(13.3, 12.9)	(21.4, 21.0)
13	(4.9, 4.5)	(7.9, 7.5)	(12.9, 12.6)	(21.0, 20.7)
14	(4.5, 4.2)	(7.5, 7.2)	(12.6, 12.3)	(20.7, 20.4)

#### ACKNOWLEDGMENT

We would like to thank Matthew Kinsey, Ryan Sawyer, Kate Tallaksen, and Richard Shaner for their valued contributions to the various research topics and modeling efforts comprising this work.

ROC Curves over SIR Bins for Dataset: DSSS, Channel

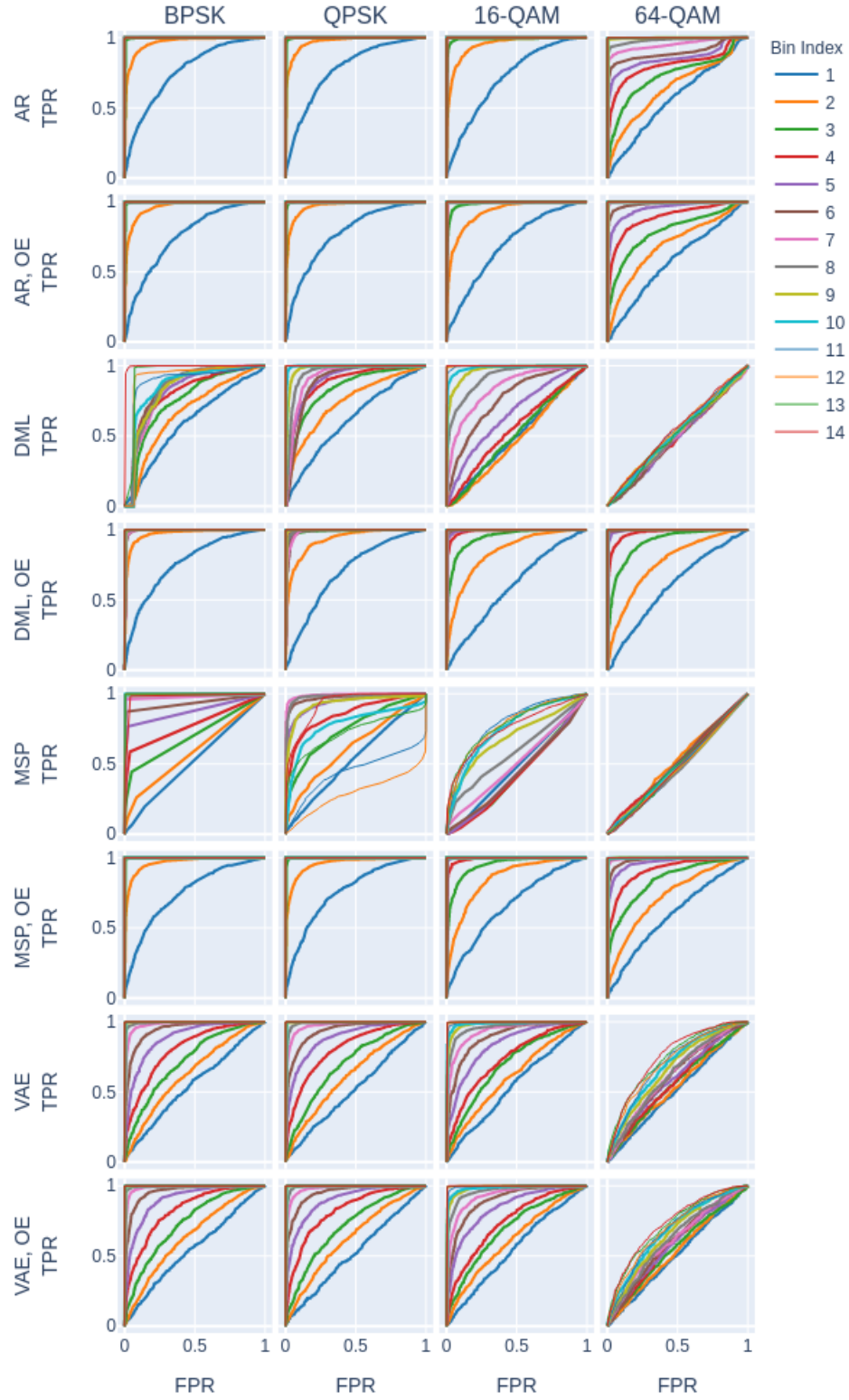


Fig. 9: All ROC curves for the DSSS weak interferer with channel effects.

## REFERENCES

- [1] 2019 Internet Statistics, Trends & Data. <https://dailywireless.org/internet/usage-statistics/>, 2002. Accessed: 2021-05-18.
- [2] Daniel Chew, Andrew L. Adams, and Jason Uher. *Wireless Coexistence: Standards, Challenges, and Intelligent Solutions*. IEEE Standards Association, 2021.
- [3] Ramakrishna Gummadi, David Wetherall, Ben Greenstein, and Srinivasan Seshan. Understanding and Mitigating the Impact of RF Interference on 802.11 Networks. *SIGCOMM Comput. Commun. Rev.*, 37(4):385–396, August 2007.
- [4] Souvik Sen, Naveen Santhapuri, Romit Roy Choudhury, and Srihari Nelakuditi. Successive Interference Cancellation: A Back-of-the-Envelope Perspective. In *Proceedings of the 9th ACM SIGCOMM Workshop on Hot Topics in Networks*, Hotnets-IX, New York, NY, USA, 2010. Association for Computing Machinery.
- [5] Bassant Selim, Sami Muhaidat, Paschalis C. Sofotasios, Arafat Al-Dweik, Bayan S. Sharif, and Thanos Stouraitis. Radio-Frequency Front-End Impairments: Performance Degradation in Nonorthogonal Multiple Access Communication Systems. *IEEE Vehicular Technology Magazine*, 14(1):89–97, 2019.
- [6] Pinchieh Huang and Yumin Lee. Adaptive Decision Feedback Orthogonality Restoration Filter for Windowed OFDM. In *IEEE 54th Vehicular Technology Conference. VTC Fall 2001. Proceedings (Cat. No.01CH37211)*, volume 2, pages 1106–1110 vol.2, 2001.
- [7] IEEE Standard for Information Technology–Telecommunications and Information Exchange between Systems - Local and Metropolitan Area Networks–Specific Requirements - Part 11: Wireless LAN Medium Access Control (MAC) and Physical Layer (PHY) Specifications. *IEEE Std 802.11-2020 (Revision of IEEE Std 802.11-2016)*, pages 1–4379, 2021.
- [8] Ian Goodfellow, Yoshua Bengio, and Aaron Courville. *Deep Learning*. MIT Press, 2016. <http://www.deeplearningbook.org>.
- [9] Timothy J O’Shea, Johnathan Corgan, and T. Charles Clancy. Convolutional Radio Modulation Recognition Networks, 2016.
- [10] Krishna Karra, Scott Kuzdeba, and Josh Petersen. Modulation Recognition using Hierarchical Deep Neural Networks. *2017 IEEE International Symposium on Dynamic Spectrum Access Networks (DySPAN)*, pages 1–3, 2017.
- [11] S. Rajendran, Wannes Meert, D. Giustiniano, Vincent Lenders, and S. Pollin. Deep Learning Models for Wireless Signal Classification With Distributed Low-Cost Spectrum Sensors. *IEEE Transactions on Cognitive Communications and Networking*, 4:433–445, 2018.
- [12] Hao-Hsuan Chang, Hao Song, Yang Yi, Jianzhong Zhang, Haibo He, and Lingjia Liu. Distributive Dynamic Spectrum Access Through Deep Reinforcement Learning: A Reservoir Computing-Based Approach. *IEEE Internet of Things Journal*, 6(2):1938–1948, 2019.
- [13] Pallavi K. Tathe and Manish Sharma. Dynamic Actor-Critic: Reinforcement Learning Based Radio Resource Scheduling for LTE-Advanced. In *2018 Fourth International Conference on Computing Communication Control and Automation (ICCUBEA)*, pages 1–4, 2018.
- [14] Guansong Pang, Chunhua Shen, Longbing Cao, and Anton Van Den Hengel. Deep Learning for Anomaly Detection. *ACM Computing Surveys*, 54(2):1–38, Apr 2021.
- [15] Dan Hendrycks and Kevin Gimpel. A Baseline for Detecting Misclassified and Out-of-Distribution Examples in Neural Networks, 2018.
- [16] Dan Hendrycks, Mantas Mazeika, and Thomas Dietterich. Deep Anomaly Detection with Outlier Exposure, 2019.
- [17] Engkarat Techapanurak and Takayuki Okatani. Practical Evaluation of Out-of-Distribution Detection Methods for Image Classification, 2021.
- [18] Jie Ren, Peter J. Liu, Emily Fertig, Jasper Snoek, Ryan Poplin, Mark A. DePristo, Joshua V. Dillon, and Balaji Lakshminarayanan. Likelihood Ratios for Out-of-Distribution Detection, 2019.
- [19] Jung Shim. *Wireless Technology: Applications, Management, and Security*, volume 44. 01 2009.
- [20] Kaiming He, X. Zhang, Shaoqing Ren, and Jian Sun. Identity Mappings in Deep Residual Networks. *ArXiv*, abs/1603.05027, 2016.
- [21] K. He, X. Zhang, S. Ren and J. Sun. Deep Residual Learning for Image Recognition. 2015.
- [22] Sergey Zagoruyko and Nikos Komodakis. Wide Residual Networks. *ArXiv*, abs/1605.07146, 2016.
- [23] Nitish Srivastava, Geoffrey E. Hinton, A. Krizhevsky, Ilya Sutskever, and R. Salakhutdinov. Dropout: A Simple Way to Prevent Neural Networks from Overfitting. *J. Mach. Learn. Res.*, 15:1929–1958, 2014.
- [24] Fisher Yu and Vladlen Koltun. Multi-Scale Context Aggregation by Dilated Convolutions. In *International Conference on Learning Representations (ICLR)*, May 2016.
- [25] Aaron Van Oord, Sander Dieleman, Heiga Zen, Karen Simonyan, Oriol Vinyals, Alex Graves, Nal Kalchbrenner, Andrew Senior, and Koray Kavukcuoglu. WaveNet: A Generative Model for Raw Audio, 2016.
- [26] Yair Movshovitz-Attias, Alexander Toshev, Thomas K. Leung, Sergey Ioffe, and Saurabh Singh. No Fuss Distance Metric Learning using Proxies, 2017.
- [27] Florian Schroff, Dmitry Kalenichenko, and James Philbin. FaceNet: A Unified Embedding for Face Recognition and Clustering. *2015 IEEE Conference on Computer Vision and Pattern Recognition (CVPR)*, Jun 2015.
- [28] Sungyeon Kim, Dongwon Kim, Minsu Cho, and Suha Kwak. Proxy Anchor Loss for Deep Metric Learning, 2020.
- [29] Charu C. Aggarwal, Alexander Hinneburg, and Daniel A. Keim. On the Surprising Behavior of Distance Metrics in High Dimensional Space. In *Database Theory*, pages 420–434. Springer Berlin Heidelberg, 2001.
- [30] Peter Julian Cayton and Dennis Mapa. Time-Varying Conditional Johnson SU Density in Value-at-



- Risk Methodology. *Philippine Review of Economics*, 51(1):23–44, 2015.
- [31] Ilya Loshchilov and Frank Hutter. Fixing Weight Decay Regularization in Adam. *CoRR*, abs/1711.05101, 2017.
  - [32] I. Loshchilov and F. Hutter. SGDR: Stochastic Gradient Descent with Restarts. *CoRR*, abs/1608.03983, 2016.
  - [33] Diederik P Kingma and Max Welling. Auto-Encoding Variational Bayes, 2013.
  - [34] Danilo Jimenez Rezende, Shakir Mohamed, and Daan Wierstra. Stochastic Backpropagation and Approximate Inference in Deep Generative Models, 2014.
  - [35] Carl Doersch. Tutorial on Variational Autoencoders, 2016.
  - [36] David M. Blei, Alp Kucukelbir, and Jon D. McAuliffe. Variational Inference: A Review for Statisticians. *Journal of the American Statistical Association*, 112(518):859–877, Feb 2017.
  - [37] Taoli Cheng, Jean-François Arguin, Julien Leissner-Martin, Jacinthe Pilette, and Tobias Golling. Variational Autoencoders for Anomalous Jet Tagging, 2021.
  - [38] Irina Higgins, Loic Matthey, Arka Pal, Christopher Burgess, Xavier Glorot, Matthew Botvinick, Shakir Mohamed, and Alexander Lerchner.  $\beta$ -VAE: Learning Basic Concepts with a Constrained Variational Framework. November 2016.
  - [39] Christopher P. Burgess, Irina Higgins, Arka Pal, Loic Matthey, Nick Watters, Guillaume Desjardins, and Alexander Lerchner. Understanding Disentangling in  $\beta$ -VAE, 2018.
  - [40] Aaron Van Oord, Nal Kalchbrenner, and Koray Kavukcuoglu. Pixel Recurrent Neural Networks. In Maria Florina Balcan and Kilian Q. Weinberger, editors, *Proceedings of The 33rd International Conference on Machine Learning*, volume 48 of *Proceedings of Machine Learning Research*, pages 1747–1756, New York, New York, USA, 20–22 Jun 2016. PMLR.
  - [41] Christopher M. Bishop. Novelty Detection and Neural Network Validation, 1994.
  - [42] Eric T. Nalisnick, Akihiro Matsukawa, Y. Teh, Dilan Görür, and Balaji Lakshminarayanan. Do Deep Generative Models Know What They Don’t Know? *ArXiv*, abs/1810.09136, 2019.
  - [43] Shaojie Bai, J. Zico Kolter, and Vladlen Koltun. An Empirical Evaluation of Generic Convolutional and Recurrent Networks for Sequence Modeling. *ArXiv*, abs/1803.01271, 2018.
  - [44] Christopher M. Bishop. Mixture Density Networks. Technical report, 1994.